This is the accepted manuscript of the article that appeared in final form in **Renewable Energy** 133 : 354-366 (2019), which has been published in final form at https://doi.org/10.1016/j.renene.2018.10.009. © 2018 Elsevier under CC BY-NC-ND license (http://creativecommons.org/licenses/by-nc-nd/4.0/)

Variable speed wind turbine control scheme using a robust wind torque estimation

Oscar Barambones, Jose A. Cortajarena, Isidro Calvo, Jose M. Gonzalez de Durana, Patxi Alkorta and A. Karami-Mollaee*
Automatic Control and System Engineering Departament
University of the Basque Country. UPV/EHU
∗ Hakim Sabzevari University, Sabzevar, Iran
Nieves cano 12. 1006 Vitoria. (SPAIN)
oscar.barambones@ehu.es

Abstract

This work proposes a robust controller for a variable speed wind turbine system with a doubly feed induction generator. The controller aims at tracking the optimal speed of the wind turbine so that extracts the maximum power from the wind. Also, a robust aerodynamic torque observer is proposed in order to avoid the use of wind speed sensors. This torque observer allows to estimate the aerodynamic torque to be used by the controller in order to calculate the value of the optimal reference speed for the wind turbine. The vector control theory is applied in the present approach, and thereby the stator flux-oriented control is used for controlling the speed of the wind turbine generator. The proposed robust control law is based on sliding mode control theory, which has proved to provide good performance under system uncertainties.

The stability of the proposed controller under disturbances and parameter uncertainties has been analyzed using the Lyapunov stability theory. Finally, real time experimental results show that, on the one hand, the proposed controller provides high-performance dynamic characteristics, and on the other hand, this scheme is robust with respect to the uncertainties that usually appear in this kind of systems.

Keywords: Renewable Energy; Wind Energy; Sliding Mode Observer; Sliding Mode Control; DFIG; Lyapunov Stability.

1. Introduction

There have been amazing improvements in wind energy extraction during the last decades. There are three main factors that explain this development. First, the decline of fossil fuel reserves and the pollution they generate. This scenario stimulated the research in alternative sources of energy like photovoltaic energy and wind energy. Second, wind energy can be found anywhere on the Earth and, in some locations, presenting a considerable density of energy. Third, some governments promoted its development for geostrategic reasons.

As a result, the wind power capacity installed has been increased intensively throughout the last decades. As a matter of example, the worldwide installed wind power capacity was about 7480 MW in 1997 whereas in the year 2017 there was around 487 GW. During the first years of the period from 1997 to 2016 the wind capacity was increased at the rate of 2000 MW per year. However, the annual growth rate increased significantly to reach a top of 64 GW, in year 2015, keeping slightly lower during the year 2016 at 55 GW. The increment of year 2016 amounts around 12% of the total wind power capacity installed worldwide and is the second largest to date just below the maximum of 2015. A significant decline in the Chinese market, following a very strong 2015, was responsible for most of the market contraction. Even so, China retained its lead for new installations, followed distantly by the United States and Germany, with India passing Brazil. Others in the top 10 for additions were France, Turkey, the Netherlands, the United Kingdom and Canada.

In 2016, China (ranked first country for additions) added 23.4 GW of wind energy, approaching its total installed capacity to 169 GW. China accounted for one-third of the total global capacity by the end of this year. However, new installations were down 24% relative to 2015, when the top growth rate was observed. The United States, ranked second for additions (8.2 GW), had a cumulative capacity of 82.1 GW at the end of 2016. Regarding energy generation the United States produced 226.5 TWh which was only 6% below China, during 2016. Germany again was the largest European market, and the third in the world, increasing operating wind power capacity by almost 5 GW for a total of 49.5 GW [1].

Therefore, wind energy for electric power generation is an area of research interest. Nowadays, the emphasis is given to the cost-effective utilization of this energy aiming at ensuring quality and reliability in the electricity delivery. Variable speed wind turbines (VSWT) are continuously increasing their market share. This kind of turbines allow to track the changes in the speed of the wind by adapting the shaft speed and thus maintaining the optimal power generation. However, a VSWT needs an adequate control system in order to operate at the optimal power efficiency [2], [3], [4], [5], [6].

The control systems for variable speed wind turbines may benefit from Doubly Feed Induction Generators (DFIG), since they allow maximizing wind power extraction. Vector control techniques are frequently adopted for that purpose. This kind of controllers ease achieving these objectives: (1) regulating the rotor speed in order to maximize the extracted power, (2) keeping constant the frequency of the output voltage at the DFIG stator, and (3) governing the reactive power extracted from the DFIG [7], [8], [9], [10].

The controller is responsible for carrying the turbine rotor speed into the desired optimal speed that maximizes the active power extracted from the wind, despite system uncertainties and wind velocity variations [11], [12], [13]. This paper explores a new approach for variable speed wind turbines based on a robust speed control method. The proposed robust control is based on sliding mode control theory, which has proved to present a good behaviour for systems subjected to uncertainties. Moreover, this kind of controllers are adequate for real time applications when limited computational resources are available, since it presents low computational costs [14], [15].

In order to calculate the optimal rotor speed, the wind speed value should be measured or estimated [16], [17], [18], [19]. This is precisely one of the contributions of this work when compared with our previous works [20] [21]. In this new paper an aerodynamic torque observer is proposed so that the control relies on the estimated aerodynamic torque rather than the wind speed measurements. In our previous research, sensors were always used to obtain the wind speed in order to calculate the reference speed for the turbine. Also, this work validates experimentally the combination of the robust control scheme for wind speed control with the proposed torque observer. For that purpose, different experiments were developed over a test bench specifically designed and constructed. The analysis of the experimental results, obtained at several operational conditions, guarantees a satisfactory behaviour.

2. System modelling

The capacity of a wind turbine for extracting power from the wind depends of three major factors: (1) the available power of the wind, (2) the power curve of the wind turbine, and (3) the ability to respond to wind fluctuations. The mechanical power produced by the wind is given by the following expression [22], [23]:

$$P_m(v, \lambda, \beta) = \frac{1}{2} C_p(\lambda, \beta) \rho \pi R^2 v^3 \tag{1}$$

where the radius of the rotor is R, the density of the air is ρ, the wind velocity is v, the wind turbine power coefficient is C_p, the pitch angle is β and, finally, λ is the tip-speed ratio, given by the following expression:

$$\lambda = \frac{R\,w}{v} \tag{2}$$

in which w represents the speed of the turbine rotor. This expression shows that, assuming a constant value for the rotor speed, the variation at the wind speed produce changes in the tip-speed ratio, since it modifies the power coefficient C_p, and, consequently, the power extracted from the wind turbine. Thus, the optimal tip-speed ratio, which extracts the maximum power output, could be kept constant by maintaining the ratio between the rotor speed and the wind speed.

The torque generated by the wind turbine can be obtained by combining expressions (1) and (2) into:

$$T_m(v, \lambda, \beta) = \frac{P_m(v, \lambda, \beta)}{w} = \frac{1}{2} C_p(\lambda, \beta) \rho \pi \frac{R^3}{\lambda} v^2 \tag{3}$$

In a simplified way, typical wind power generation systems are composed by the following three elements: (1) turbine, which converts wind energy into mechanical energy, (2) gearbox, which increases the speed and decreases the torque, and (3) generator, which produces electrical energy from mechanical energy.

The input wind torque T_m drives the wind turbine rotor to spin at the speed w, producing a transmission output torque T_t which is used to fed the generator. The shaft torque at the generator T_e produces an angular velocity of w_e. Note that, the rotor and generator speeds may differ since they are related by a gearbox.

The mechanical behaviour of the wind power system may be characterized by the following equations[24]:

$$\begin{aligned} J_m\dot{w} + B_m w &= T_m - T \quad (4)\\ J_e\dot{w}_e + B_e w_e &= T_t - T_e \quad (5)\\ T_t w_e &= T w \quad (6)\end{aligned}$$

where J_e and J_m are the moments of inertia of both generator and turbine, B_e and B_m represent respectively the viscous friction coefficients of generator and turbine, T_m is the torque generated by the wind at the turbine, the torque at the transmission shaft before and after the gear box are represent by T and T_f respectively and T_e is the torque produced by the generator when spinning at angular velocity w_e.

The angular velocities of both generator, w_e, and turbine, w, are related by the gear ratio η:

$$\gamma = \frac{w_e}{w} \quad (7)$$

The following expression, which represents the model of the wind system, can be obtained by combining equations (4), (5), (6) and (7):

$$J\dot{w} + Bw = T_m - \gamma T_e \quad (8)$$

where

$$\begin{aligned} J &= J_m + \gamma^2 J_e \quad (9)\\ B &= B_m + \gamma^2 B_e \quad (10)\end{aligned}$$

3. Aerodynamic torque observer

This section proposes an aerodynamic torque estimator aimed at avoiding the wind speed measurements needed to calculate the optimal turbine speed that extracts the maximum power from the wind.

The aerodynamic torque may be considered as a quasi-constant signal for a time interval since the variation of the mean value of the wind does not change quickly and, moreover, the wind turbine system has some inertia that may absorb these variations. Accordingly, the state space equations for the wind turbine system (8) may be rewritten as:

$$\begin{aligned} \dot{w} &= \frac{1}{J}\left(T_m - Bw - \gamma T_e\right)\\ \dot{T}_m &= 0 \quad (11)\end{aligned}$$

Since the aerodynamic torque T_m is taken as a quasi-constant signal, it can be regarded as the slow component of the system. According to singular perturbation theory [25], the stability of a system can be proved if the asymptotic stability of the fast component (i.e. rotor speed) is ensured. Thereafter, for the reduced system, the convergence of the slow component (i.e. aerodynamic torque) can be achieved when the estimation error for the rotor speed is null.

The next observer, based on sliding mode theory, is proposed:

$$\begin{aligned} \dot{\hat{w}} &= \frac{1}{J}\left(\hat{T}_m - Bw - \gamma T_e\right) + k_{w_1} e_w + h_1 \operatorname{sgn}(e_w) \\ \dot{\hat{T}}_m &= k_{w_2} e_w + h_2 \operatorname{sgn}(e_w) \end{aligned} \tag{12}$$

where the observation error of the turbine speed is $e_w = w - \hat{w}$, and h_1, h_2, k_{w_1} k_{w_2} are the parameters of the observer, which should be chosen greater than 0.

The observation error dynamics for the rotor speed may be obtained by subtracting eqn.(12) from eqn.(11):

$$\begin{aligned} \dot{e}_w &= \frac{1}{J} e_T - k_{w_1} e_w - h_1 \operatorname{sgn}(e_w) \\ \dot{e}_T &= -k_{w_2} e_w - h_2 \operatorname{sgn}(e_w) \end{aligned} \tag{13}$$

where $e_T = T_m - \hat{T}_m$

The stability of the fast component can be proved by means of the following Lyapunov candidate function.

$$V = \frac{1}{2} e_w^2 \tag{14}$$

The derivative of this function with respect to time is:

$$\dot{V} = e_w \dot{e}_w \tag{15}$$

$$= e_w \left(\frac{1}{J} e_T - k_{w_1} e_w - h_1 \operatorname{sgn}(e_w)\right) \tag{16}$$

$$= \frac{1}{J} e_w e_T - h_1 |e_w| - k_{w_1} e_w^2 \tag{17}$$

The next condition must be satisfied to ensure that $\dot{V}$ is a negative definite function:

$$h_1 \geq \left|\frac{1}{J} e_T\right| - k_{w_1} |e_w| + \eta_w \ , \quad \eta_w > 0 \tag{18}$$

Accordingly,

$$\dot{V} \leq -\eta_w |e_w| \tag{19}$$

From (19) it may be deduced that the equilibrium point, $e_w = 0$, is asymptotically stable. Also, this equation shows that the equilibrium point $e_w = 0$ is reached in finite time since:

$$t_{reach} \leq \frac{e_w(t=0)}{\eta_w} \tag{20}$$

From (13) it may be noticed that when the equilibrium point is reached, i.e. $e_w = 0$ and $\dot{e}_w = 0$, the dynamics of the error observer is comparable to the following reduced-order subsystem:

$$0 = \frac{1}{J} e_L - h_1 \operatorname{sgn}(e_w) \quad (21)$$

$$\dot{e}_T = -h_2 \operatorname{sgn}(e_w) \quad (22)$$

Using the above equations it can be inferred:

$$\dot{e}_T = \frac{-1}{J} \frac{h_2}{h_1} e_T \quad (23)$$

In conclusion, the aerodynamic torque estimation error converges to zero if the observer gains h_1, h_2 k_{w_1} and k_{w_2} are appropriately selected. Accordingly, the estimated states $\hat{w}_m$, $\hat{T}_m$ converge to the real states w_m, T_L as t tends to infinity. So, the aerodynamic torque may be obtained from the sliding mode observer given by eqn.(12).

4. Wind turbine generator control

In this VSWT system a DFIG is employed, which is fed from the rotor and the stator of the generator. The rotor is fed by means of a variable frequency converter (VFC) and the stator is directly connected to the grid. This system is required to deliver electrical power to the grid over a wide range of operation (from subsynchronous to supersynchronous speed) while ensuring constant values for voltage and frequency. For that purpose, the active power flow between the rotor circuit and the grid should be controlled in magnitude and direction. This is achieved by two four-quadrant IGBT PWM converters, one for the rotor-side (RSC), and another for the grid-side (GSC), connected back-to-back by a DC-link capacitor [26].

In order to extract the maximum power from the wind, improving the efficiency, the shaft speed of the generator must be regulated in order to obtain the optimal tip-speed ratio λ_{opt}. This optimal tip-speed ratio maximizes the value of the power coefficient $C_{p_{max}}$ and, therefore, the generated power[13]. In other words, there is a unique value for the wind turbine speed that, for a particular wind speed, maximizes wind power extraction. The maximum value of the power coefficient curves versus tip-speed ratio is represented by λ_{opt}. This value depends of the turbine design characteristics.

In this scenario, the use of the estimated aerodynamic torque $\hat{T}_m$ allows calculating the turbine speed reference without using wind speed measurements.

Equations (1) and (2) may be combined to express the wind turbine power as a function of the turbine speed:

$$P_m(w, \lambda, \beta) = \frac{1}{2} C_p(\lambda, \beta) \rho \pi R^2 \left(\frac{Rw}{\lambda} \right)^3 = k_w(\lambda, \beta) \cdot w^3 \quad (24)$$

where

$$k_w = \frac{1}{2} C_p(\lambda, \beta) \rho \pi \frac{R^5}{\lambda^3}$$

Thus, the value for the maximum power generation can be calculated with eqn.(24):

$$P_{m_{opt}} = T_{m_{opt}} \cdot w_{opt} = k_{w_{opt}} \cdot w_{opt}^3 \tag{25}$$

where

$$k_{w_{opt}} = \frac{1}{2}\, C_p(\lambda_{opt}, \beta)\, \rho\, \pi \frac{R^5}{\lambda_{opt}^3}$$

being λ_{opt} the value of λ that yields the maximum power coefficient C_p.

Hence, the optimal speed for the rotor can be obtained from eqn.(25) and the estimated aerodynamic torque (12):

$$w_{opt} = \sqrt{\frac{\hat{T}_m}{k_{w_{opt}}}} \tag{26}$$

Figure 1 shows the power characteristic curves for the turbine employed in this study, namely, several curves for wind speed values ranging from 5 m/s to 16.2 m/s. It should be noted that eqn.(26) yields the points of the red curve of figure 1 between B and C since they are the maximum values of the turbine output power.

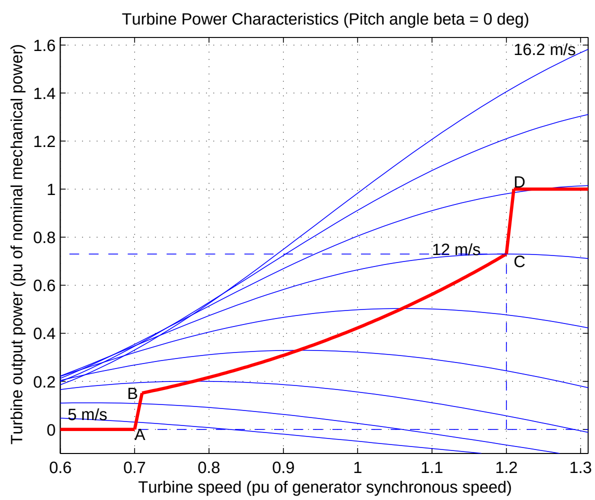

Figure 1: Turbine Power Characteristics

Therefore, a control scheme aimed at regulating the wind turbine speed in order to track the optimal wind speed is required. This controller should be able to maximize the power coefficient and, therefore, to extract the maximum power from the wind, increasing the wind turbine performance. Consequently, the turbine speed controller should be adequately designed in order to track the optimal reference speed for the turbine $w^* = w_{opt}$.

For this purpose, the current of the rotor is typically regulated using the stator-flux oriented reference frame [27]. In this frame, the d-axis is aligned with the stator flux linkage vector ψ_s, so that ψ_{ds}=ψ_s and ψ_{qs}=0 and accordingly the next model is obtained [28]:

$$i_{qs} = \frac{L_m i_{qr}}{L_s} \tag{27}$$

$$i_{ds} = \frac{L_m(i_{ms} - i_{dr})}{L_s} \tag{28}$$

$$T_e = \frac{L_m i_{ms} i_{qr}}{L_s} \tag{29}$$

$$Q_s = \frac{3}{2}\frac{w_s L_m^2 i_{ms}(i_{ms} - i_{dr})}{L_s} \tag{30}$$

$$v_{dr} = r_r i_{dr} + \sigma L_r \frac{di_{qr}}{dt} - s w_s \sigma L_r i_{qr} \tag{31}$$

$$v_{qr} = r_r i_{qr} + \sigma L_r \frac{di_{qr}}{dt} \tag{32}$$

$$+ s w_s \left(\frac{\sigma L_r i_{dr} + L_m^2 i_{ms}}{L_s}\right) \tag{33}$$

where

$$i_{ms} = \frac{v_{qs} - r_s i_{qs}}{w_s L_m} \tag{34}$$

$$\sigma = 1 - \frac{L_m^2}{L_s L_r} \tag{35}$$

Given that the grid is connected to the stator and considering that the the stator resistance has low influence, the value of the magnetizing current of the stator i_{ms} can be approximated as a constant value [26]. Accordingly, the electromagnetic torque of the DFIG can be modeled as:

$$T_e = K_T i_{qr} \tag{36}$$

where K_T is a torque constant defined as:

$$K_T = \frac{L_m i_{ms}}{L_s} \tag{37}$$

From equations (8) and (36) it may be observed that the q-axis rotor current component i_{qr} can be used to control the speed of the wind turbine. Equation (30) shows that the d-axis component of the rotor current i_{dr} could be used to govern the reactive power at the stator Q_s. Accordingly, the values for the currents i_{qr} and i_{dr} can be obtained from the reference values provided from w_r and Q_s.

The following differential equation for the system speed has been inferred from equations (8) and (36):

$$\dot{w} = \frac{1}{J}\left(T_m - \gamma K_T i_{qr} - B w\right) \tag{38}$$

$$= -aw + f - b i_{qr} \tag{39}$$

being the parameters f, a and b defined as:

$$f = \frac{T_m}{J}, \quad a = \frac{B}{J}, \quad b = \frac{\gamma K_T}{J}; \tag{40}$$

Now, the previous equation (39) will be considered taking into account some uncertainties:

$$\dot{w} = -(a + \triangle a)w + (f + \triangle f) - (b + \triangle b)i_{qr} \tag{41}$$

where the terms $\triangle b$, $\triangle a$ and $\triangle f$ take into account the uncertainties at the parameters b, a and f respectively.

Let be defined the speed tracking error as:

$$e(t) = w(t) - w^*(t) \tag{42}$$

where the command for the rotor speed is w^*.

Calculating the time derivative of the previous equation it is obtained:

$$\dot{e}(t) = \dot{w} - \dot{w}^* = -a\, e(t) + u(t) + d(t) \tag{43}$$

where the signal $u(t)$ groups the know terms,

$$u(t) = f(t) - b\, i_{qr}(t) - a\, w^*(t) - \dot{w}^*(t) \tag{44}$$

and the signal $d(t)$ groups the uncertainty terms,

$$d(t) = -\triangle a\, w(t) + \triangle f(t) - \triangle b\; i_{qr}(t) \tag{45}$$

The system uncertainties, described above, may be compensated by a sliding control scheme. Note that in sliding mode control theory the sliding gain must be selected in order to satisfy the sliding condition [29]. Hence, the value for the sliding gain should be chosen carefully to meet the previous condition.

The proposed sliding variable $S(t)$ is defined with an integral component as:

$$S(t) = e(t) + \int_0^t (k + a)e(\tau)\, d\tau \tag{46}$$

where k is a positive constant gain.

Regarding the sliding surface, it has been defined as:

$$S(t) = e(t) + \int_0^t (a + k)e(\tau)\, d\tau = 0 \tag{47}$$

Also, a variable structure speed controller, aimed at controlling the wind turbine speed, has been introduced.

$$u(t) = -k\, e(t) - \beta\, \mathrm{sgn}(S) \tag{48}$$

where β is the sliding gain and $\mathrm{sgn}(\cdot)$ is the sign function.

The next assumption should be satisfied to obtain the tracking of the optimal reference speed for the wind turbine:

($\mathcal{A}\,1$) The gain β must be selected so that $\beta \geq |d(t)|$.

Note that this assumption means that the value of the system uncertainties are finite.

Theorem 1. *Considering a VSWT defined by equation (41) and assumption* ($\mathcal{A}\,1$)*. Then, the control law presented in Eqn.(48) governs the speed of the wind turbine* $w(t)$ *so that the tracking error of the wind turbine velocity* $e(t) = w(t) - w^*(t)$ *approximates to zero exponentially.*

This theorem may be proved by means of the Lyapunov stability theory.

Proof : The candidate of the Lyapunov function is defined as:

$$V(t) = \frac{1}{2}S(t)S(t) \tag{49}$$

Calculating the time derivative of the previous function:

$$\begin{aligned}
\dot{V}(t) = \quad & S(t)\dot{S}(t) \\
&= S \cdot [\dot{e} + (k+a)e] \\
&= S \cdot [(-a\,e + u + d) + (k\,e + a\,e)] \\
&= S \cdot [u + d + k\,e] \\
&= S \cdot [-k\,e - \beta\,\mathrm{sgn}(S) + d + k\,e] \\
&= S \cdot [d - \beta\,\mathrm{sgn}(S)] \\
&\leq -(\beta - |d|)|S| \\
&\leq 0
\end{aligned} \tag{50}$$

Eqns. (46), (43) and the ($\mathcal{A}\,1$) assumption were used in this proof.

Previous equations show that (1) $V(t)$ is positive-definite, (2) $\dot{V}(t)$ is negative definite and (3) $V(t)$ tends to infinity when $S(t)$ tends to infinity. From the Lyapunov direct method, it may be concluded that the equilibrium at the origin $S(t) = 0$ is globally asymptotically stable. Hence, when time tends to infinity, the sliding variable $S(t)$ goes to zero. Besides, the trajectories of this system will reach the sliding surface $S = 0$ in finite time and thereafter will remains in this surface (47). When so happens $S(t) = \dot{S}(t) = 0$ and therefore the dynamic behaviour of the tracking problem (43) is represented by the next dynamic equation:

$$\dot{S}(t) = 0 \quad \Rightarrow \quad \dot{e}(t) = -(k+a)e(t) \tag{51}$$

Therefore, taking into account that k and a are a positive constants, the speed tracking error $e(t)$ converges exponentially to zero.

Finally, the command for q-component of the current, $i^*_{qr}(t)$, can be calculated from equations (48) and (44):

$$i^*_{qr}(t) = \frac{1}{b}\left[k\,e + \beta\,\mathrm{sgn}(S) - a\,w^* - \dot{w}^* + f\right] \tag{52}$$

Therefore, the wind turbine speed regulation in order to maximize the power generation under system uncertainties can be obtained using the value for the rotor current given by the previous equation.

5. Experimental Results

This section analyses the behaviour of the proposed control scheme when the sliding mode observer developed in this paper is used, by means of several experimental tests in a real platform designed ad hoc.

5.1. Description of the platform

Figure 2 shows the block diagram of the experimental platform used for the validation of the control set up. A photography of the experimental platform is provided at figure 3.

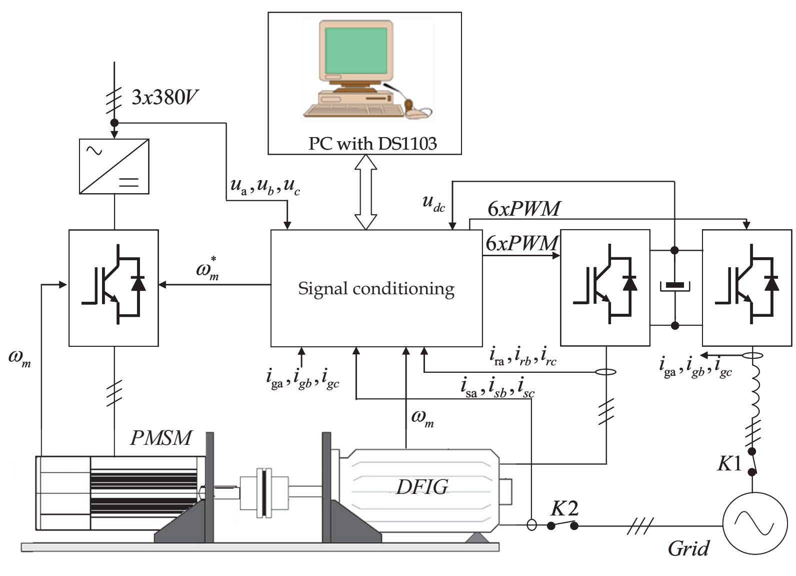

Figure 2: Block diagram of the experimental platform

The control platform displayed in figure 2 includes a PC with MatLab7/Simulink R2007a and DSControl 3.2.1 software and a dSpace DS1103 controller board, which includes a floating point PowerPC processor of 1 GHz. The proposed test bench also includes a commercial DFIG machine of 7.5 kW and 1447 rpm provided by Leroy

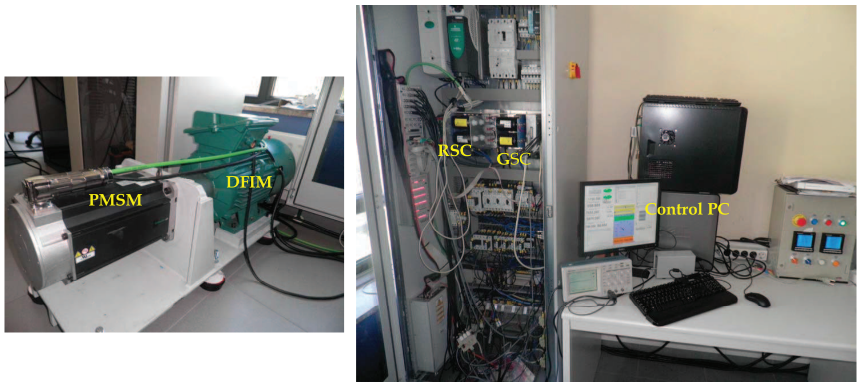

Figure 3: Photography of the experimental platform

Somer. This DFIG is connected to the grid through the rotor in a back-to-back configuration with two voltage source inverters of Dutt Power Electronics & Control. The parameters of the DFIG are indicated in Table 1.

The wind turbine has been emulated by means of a synchronous AC servo motor, namely a 10.6 kW 190U2 provided by Unimotor. The DFIG and the synchronous AC servo moto are mechanically coupled by the shaft.

The mechanical wind turbine torque values are generated using a turbine model implemented in Simulink, based on equation (3). The wind profile is used as input for the turbine model in Simulink and this model generates the torque reference for the AC servo motor. Then the AC servo motor generates the torque that moves the rotor of the DFIG. In this sense, the torque produced by a wind profile in the wind turbine is generated by means of the synchronous AC servo motor

A servo motor incremental encoder of 4096 square impulses per revolution is employed in order to measure the rotor speed.

Both rotor and stator currents are limited to their nominal values to protect the machine against over currents. All sensors used to measure currents, voltages and speed magnitudes were adapted to be connected to the DS1103 controller board. This board controls both inverters generating the SVPWM (space vector pulse width modulation) pulses. The SVPWM frequency is set at 7kHz, determining the sample period for the program execution at 143 μs. A dead time of 1 μs, which is controlled both by software and hardware, is used for the inverters. A synchronous reference frame phase-locked loop (SRF-PLL) is used for extracting the grid voltage phase, frequency and amplitude in order to synchronize the DFIG with the grid.

The grid side converter is controlled in the grid voltage reference system, imposing a DC voltage of 570V and a reactive power of 0 VAR. Conventional PI controllers have been used for this task. The analysis of this control is out of scope in this work.

The starting process begins with the grid synchronization, when this is done the K1 contactor is closed and the DC voltage bus is regulated. The voltage in the DC link must be greater than the peak value of the grid voltage, which is 540 for a grid RMS voltage of 380V. Therefore, the DC voltage is regulated to 570V. Once the DC voltage is regulated, the encoder offset is determined and the DFIG stator is synchronized with the grid, connecting after that the stator to the grid closing K2. Finally, the rotor current is regulated using the implemented controllers.

Stator Voltage	380 V
Rotor Voltage	190 V
Rated stator current	18 A
Rated rotor current	24 A
Rated speed	1447 r.p.m.@ 50 Hz
Rated torque	50 Nm
Stator resistance	0.325 Ω
Rotor resistance	0.275 Ω
Magnetizing inductance	0.0664 H
Stator leakage inductance	0.00264 H
Rotor leakage inductance	0.00372 H
Inertia moment	0.07 $Kg.m^2$

Table 1: Ratings and parameters of the DFIG (Leroy Somer).

5.2. Simulation of the DFIG and validation of the real platform

A comparison between the response of the experimental system platform and the simulation model at different speeds and load torques proves that the model used for the experimental platform is adequate since both systems produce similar results. The test has been performed during 9 seconds when changing simultaneously the speed of the DFIG from 900 rpm to 2000 rpm and the load torque from 0 to 25 Nm.

Figure 4 pictures the rotor speeds, the load torque reference and the electromagnetic torque obtained from both the simulation model and the real platform. Figure 5 depicts the power obtained from stator and rotor in both the simulation model and the experimental system platform for the specific speed and torque profiles. Finally, figure 6 shows the rotor d and q current components as well as the rotor phase current for the speed and load torque profiles used. The graphs obtained at simulation and in the experimental system platform look very similar, showing that the simulation model approximates accurately the real system. Therefore, the simulation model can be used to adjust the sliding controller and torque estimator, before implementing this control scheme at the real system platform avoiding undesirable damages.

5.3. Sliding torque estimator and optimum speed reference

In the real platform, the wind turbine can be modelled using equation (3), which determines the torque generated for the selected wind speed profile. The characteristic curves of the wind turbine model were presented in figure 1. Figure 7 shows the characteristic curves of the power coefficient $C_p(\lambda, \beta)$ for this wind turbine versus different λ and β values.

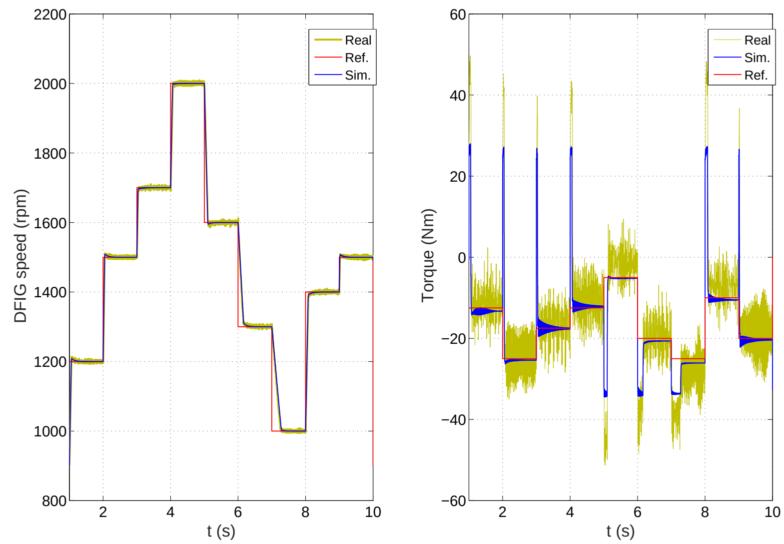

Figure 4: Real and simulated DFIG speed and torque

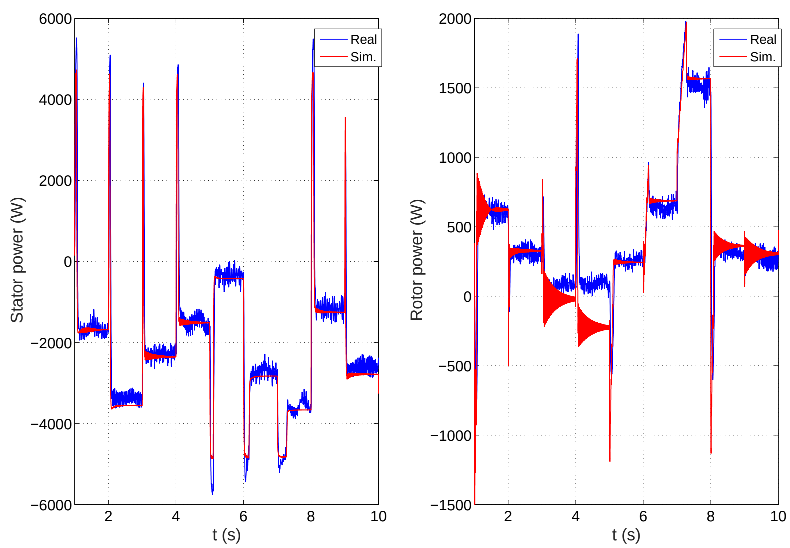

Figure 5: Real and simulated DFIG stator and rotor power for the speed and torque profile of figure 4

Next, the performance of the proposed sliding mode estimator is analysed. For this purpose, the wind turbine speed and torque values obtained at the experimental

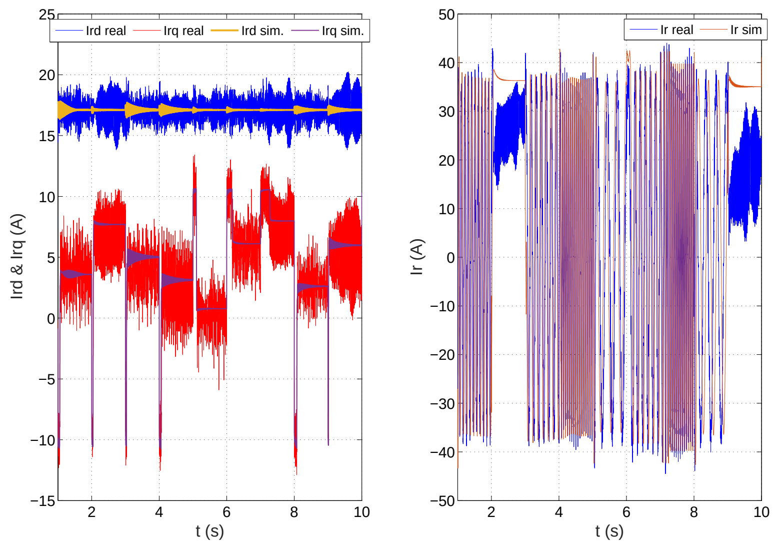

Figure 6: Real and simulated DFIG rotor d and q current components and rotor phase current for the speed and torque profile of figure 4

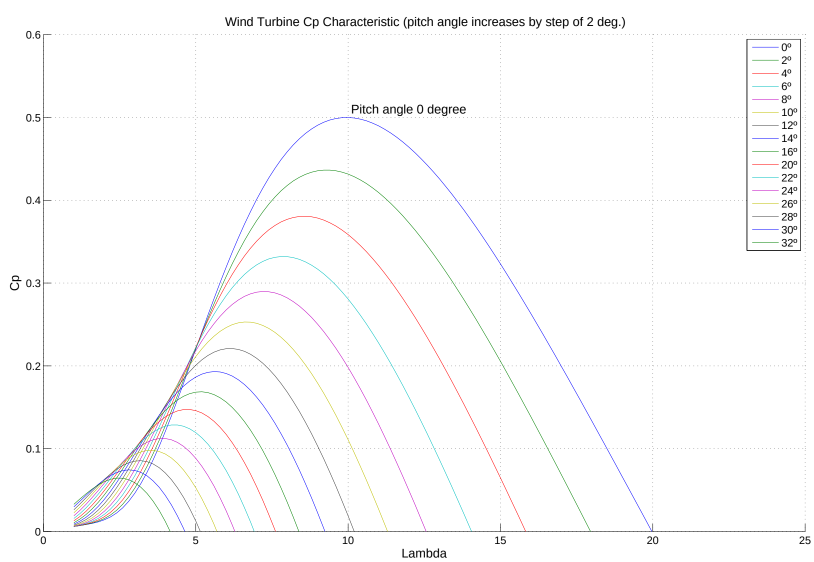

Figure 7: Wind Turbine characteristic curves for the Power Coefficient.

platform are compared with the estimated values. Both the wind turbine torque and speed were estimated with the sliding observer proposed in equation (12). The observer parameters h_1 and h_2 were firstly tuned using the simulation model and finally refined at the real platform, obtaining the following values $h_1 = 6200$ and $h_2 = 9000$.

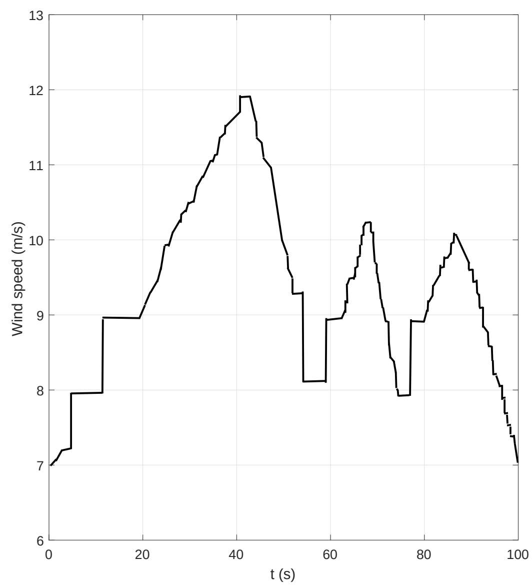

Figure 8: Wind speed profile.

Figure 8 presents the random wind speed profile selected for this experimental test. It should be noted that, although unusual, some sudden changes in the wind speed were added to analyse the dynamic performance of the observer proposed.

Figure 9 shows the DFIG real and estimated rotor speeds as well as the wind turbine torques obtained for the wind profile represented at figure 8. Comparing both the real and estimated values, it is clear that the sliding observer estimates accurately the DFIG torque and speed even when sudden wind speed variations appear, producing sudden changes at the wind turbine. The estimated torque can be used to impose the optimal speed reference to the DFIG using equation (26) and, accordingly, to maximize the power obtained.

The moment of inertia almost does not change in a wind system. However, an error in the total inertia of the system has a relevant impact in the estimation of the torque in conventional estimators, like the Luenberger observer. The sliding mode observer provides some robustness under this kind of uncertainties. Figure 10 presents the response of the observer to different wind steps changes with mismatches in the inertia value of 25%. The upper graphs of figure 10 picture the reference calculated for the optimal speed under different wind steps changes. The line marked as Ref. represents

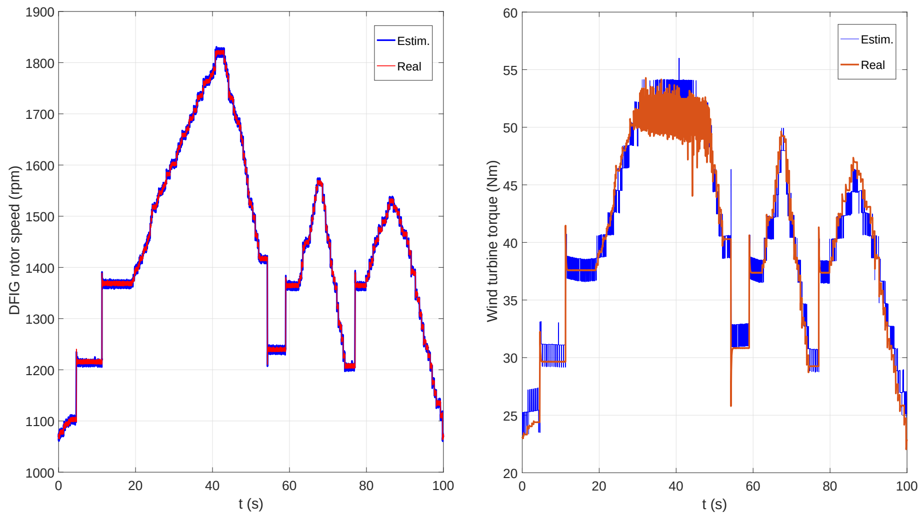

Figure 9: Real and estimated rotor speed and real and estimated wind turbine torque.

the optimal speed reference obtained from equation (2), using the wind speed and the λ_{opt} value. The other lines depict the optimal speed obtained by means of the estimated torque value, calculated from equations (12) and (26). These figures show the response of the observer for different error values of the moment of inertia: without error (blue line), +25% error (red line) and -25% error (green line). It can be appreciated that in case of error at the moment of inertia, the estimated torque and the optimal speed values degrade in the transitory for a some time. However, after a short period of time, the proposed observer behaves correctly yielding the optimal speed reference for the DFIG. The bottom graphs of this figure show the real torque produced by the wind and the estimated torque value obtained from the proposed sliding mode observer.

Figure 11 shows a comparison between the wind torque value, calculated from the wind turbine model with eqn.(3), and the wind torque value, obtained using the proposed sliding mode observer, eqn.(12), when a random wind speed profile is used as input. Both values are quite similar, hence, we can assume that the proposed observer provides a good estimation of the wind torque value. The estimated torque allows to calculate the optimal speed value, with eqn.(26), which can be compared with the optimal speed value obtained from eqn.(2). This figure also shows that the optimal speed value obtained from the proposed estimator is good enough. Finally, this figure shows the behaviour of the system when the pitch angle value changes, which avoids damages in the system caused when the power generated from the wind exceeds the DFIG maximum power. Even with these variations at the pitch angle the optimal speed value is correctly calculated.

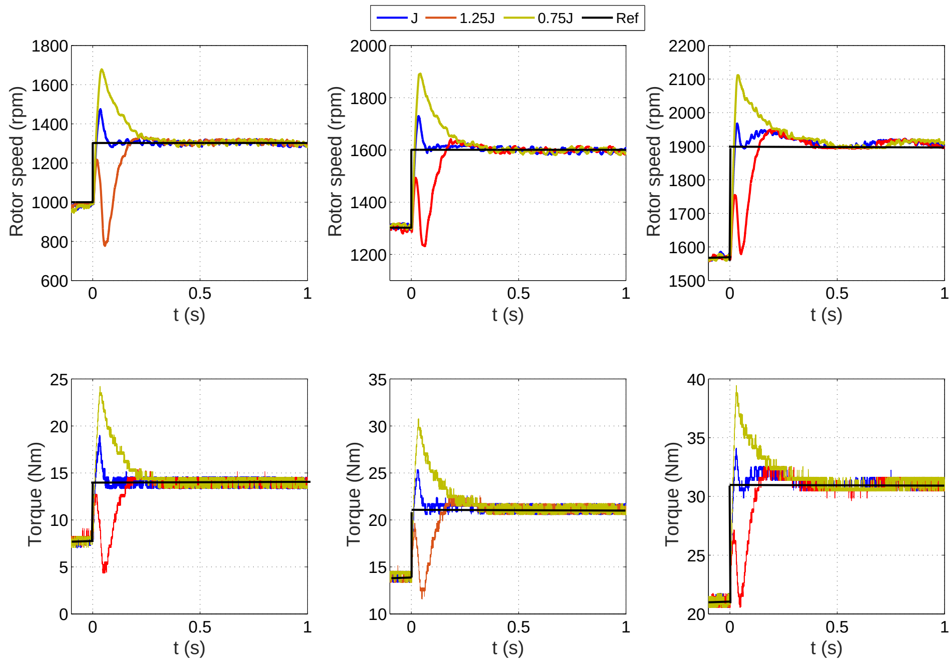

Figure 10: Proposed SMC observer performance for different wind steps changes and under different errors in the inertia moment value

5.4. Sliding Mode Control

This subsection describes the tests carried out over the experimental platform using the proposed sliding mode control and torque observer to set the optimal turbine speed. A scenario in which the wind speed varies randomly, as seen in the figure 12-a, has been selected. The chosen values for the sliding mode controller were $k = 20$ and $\beta = 100$. A fixed reactive power of 4000 VAR was used at the DFIG.

Figure 12-b compares the values of the wind torque, experimentally measured, and the sliding mode observer torque, calculated with eqn. (12). The figure shows that the proposed observer yields a good estimation of the torque value. Figure 12-c shows the optimal rotor speed obtained from equation (26) using the estimated torque value. This value is compared with the real optimal reference, obtained from equation (2) using the real wind speed. As it can be observed, the optimal rotor speed obtained by our approach is very close to the optimal wind speed value, even though in our case it was not required. Figure 12-d compares the experimental rotor speed with the reference in order to evaluate the performance of the proposed sliding mode speed control.

Figure 13 shows the stator power, the rotor power and the total power extracted for the test wind speed profile using the proposed sliding mode controller and observer.

Finally, figure 14 shows the stator and rotor currents of the DFIG for the analysed set up.

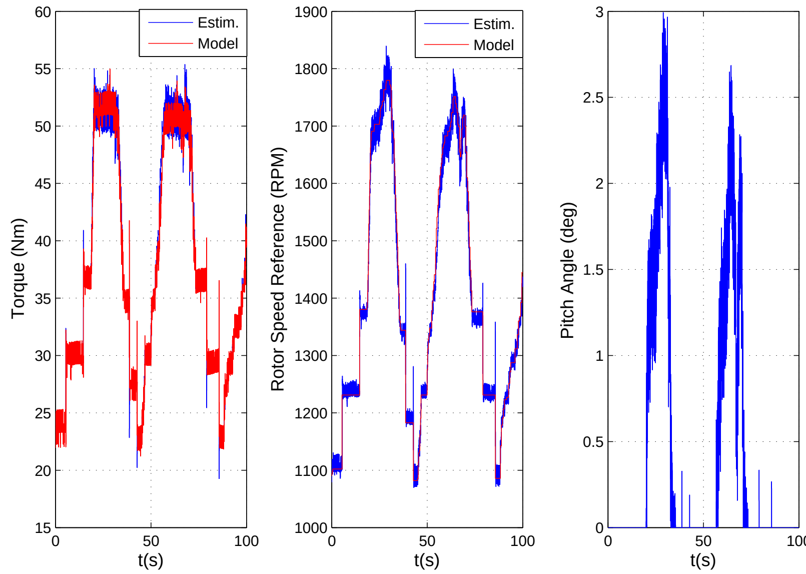

Figure 11: Turbine model torque and SMC estimated torque. Optimal rotor speed according to the turbine model and to the SMC observer. Pitch angle for the imposed torque and speed.

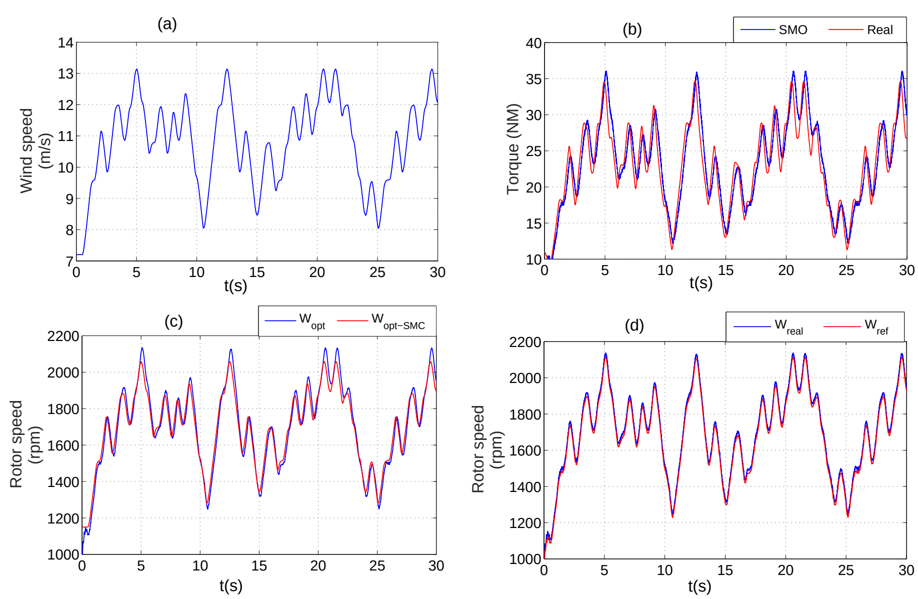

Figure 12: Performance of the SM controller and observer for a random wind profile

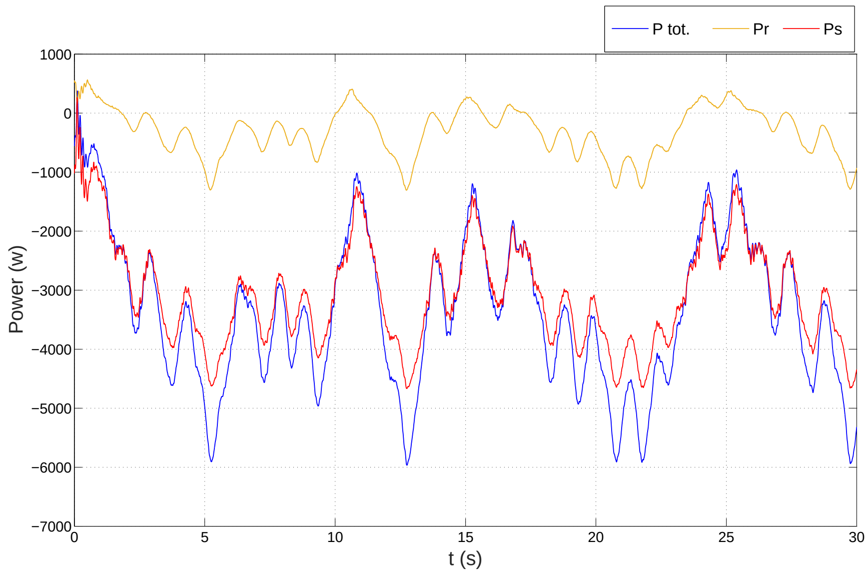

Figure 13: Stator power, the rotor power and the total power for a random wind profile

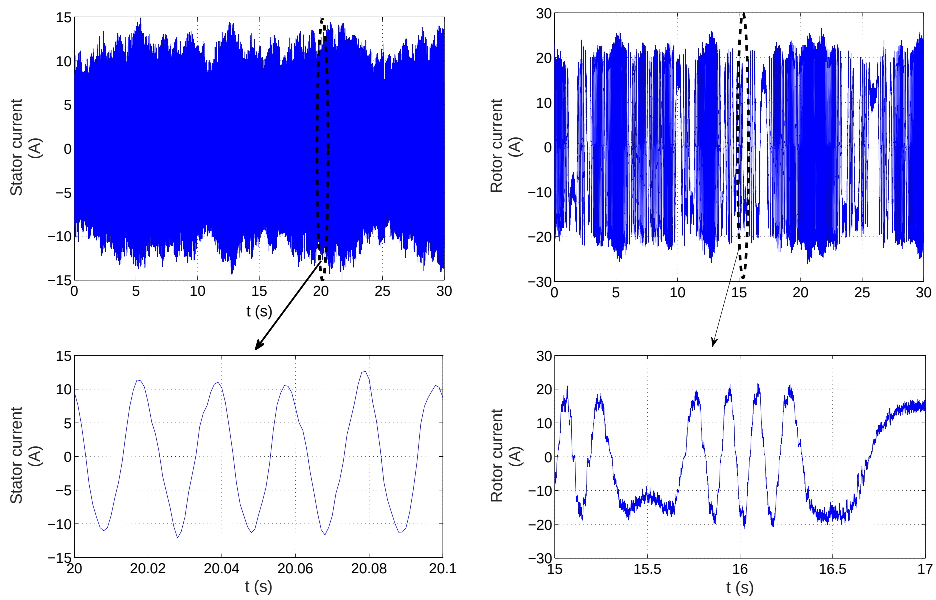

Figure 14: Stator and rotor currents for a random wind profile

5.5. *Sliding Mode Control versus PI control*

In this experimental validation, the traditional PI controller is compared with the proposed SMC in order to shown the controller performance. As it is well known, the PI controller is the most widely used controller in the industry and this controller is usually employed for comparing the new control schemes [30], [31], [32].

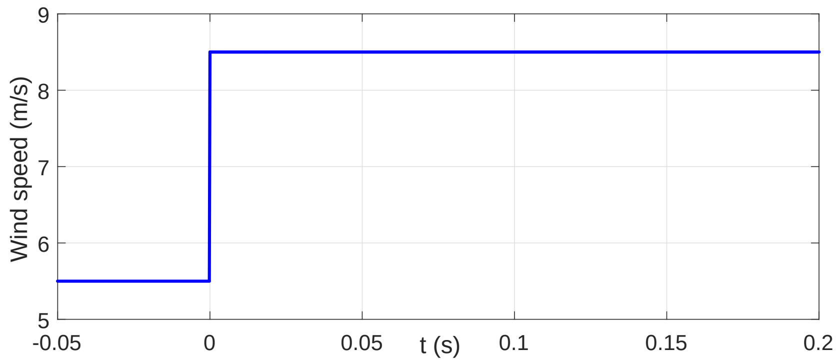

Figure 15: Wind speed step reference

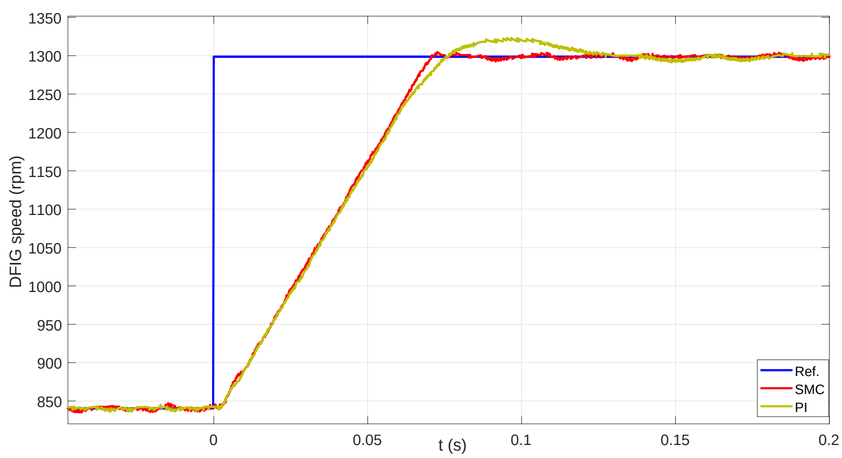

Figure 16: Rotor speed regulation using the traditional PI controller and the proposed SMC

This validation has been carried out over the real platform using the step change in the wind speed, shown in Figure 15, in order to show the controller performance under a sudden wind changes which is a exigent task for the control scheme. This wind step variation produces a change in the rotor speed reference (to follow the maximum power extraction) as it is shown in Figure 16. In the same figure the response for both controllers is also shown. The PI controller is adjusted with a bandwith of 50 rad/s and a phase margin of 75 deg. In this figure it can be observed that using the SMC controller the rotor speed tracks the reference speed that provides the maximum power extraction from the wind. Obviously due to the system mechanical inertia, the rotor speed can not track the speed changes in the reference speed but after a 0.08 s the reference speed is reached. The figure also shown that the response rate of the PID controller is similar to the response rate of the SMC controller and both controllers provides a similar rise time. However, in the PID controller an overshoot can be observed, and therefore the system takes more time to reach the reference speed, that provides the maximum power extraction, from this new wind speed value. This overshoot can be reduced decreasing the proportional action of the controller but in this case a slower response will be obtained.

6. Conclusion

This paper describes the design of a sliding mode vector control for a doubly feed induction generator drive, used in variable speed wind power generation. An integral sliding surface is proposed to relax the requirements at the acceleration, which is usually required in sliding mode schemes for speed control. The nature of the sliding control technique ensures the robustness of the control scheme under the uncertainties that may appear in real systems. The stability of the close loop for the presented scheme was analysed and proved by means of Lyapunov stability theory.

Moreover, in order to avoid wind velocity measurements, a sliding mode observer for the aerodynamic torque is proposed. This observer will be used to calculate the reference speed of the wind turbine, providing the optimal tip speed ratio for the sliding mode controller, i.e. which maximizes power extraction.

The proposed approach allows to operate a wind turbine over a wide range of values for the wind speed while optimizing power efficiency. This controller regulates the speed of the wind turbine by obtaining the optimal tip speed ratio, and consequently, producing the maximum power.

Experimental tests, developed in a real test bench which was designed and constructed ad hoc, prove that the proposed control method controls efficiently and successfully the variable speed wind turbine within a range of normal operational conditions. These tests evidence that the proposed observer provides a good estimation of the aerodynamic torque under system uncertainties and wind speed variations. Finally, experimental results also show that the speed tracking objective is achieved in order to maintain the maximum power extraction under wind speed variations and system uncertainties.

Acknowledgment

The authors are very grateful to the UPV/EHU by its support through the projects PPGA17/02 and UFI11/07 and to the Basque Government by its support through the project ELKARTEK 2017.

References

[1] Renewable energy policy network for the 21st century (REN21), Renewables 2017 Global Status Report, 2017, REN21 Secretariat. Paris (France). http://www.ren21.net/

[2] Jackson G. Njiri, Dirk Sffker. State-of-the-art in wind turbine control: Trends and challenges. Renewable and Sustainable Energy Reviews. 2016;60:377-393.

[3] Fernando A. Inthamoussou, Hernn De Battista, Ricardo J. Mantz. LPV-based active power control of wind turbines covering the complete wind speed range. Renewable Energy 2016;99:996-1007.

[4] Mahinsasa Narayana, Keith M. Sunderland, Ghanim Putrus, Michael F. Conlon. Adaptive linear prediction for optimal control of wind turbines. Renewable Energy 2017;113:895-906.

[5] Bo Yang, Tao Yu, Hongchun Shu, Yuming Zhang, Jian Chen, Yiyan Sang, Lin Jiang. Passivity-based sliding-mode control design for optimal power extraction of a PMSG based variable speed wind turbine. Renewable Energy 2018;119:577-589.

[6] Andreas Giannakis, Athanasios Karlis, Yannis L. Karnavas. A combined control strategy of a DFIG based on a sensorless power control through modified phase-locked loop and fuzzy logic controllers. Renewable Energy 2018;121:489-501.

[7] Wei Qiao, Wei Zhou, Jos M. Aller, and Ronald G. Harley Wind Speed Estimation Based Sensorless Output Maximization Control for a Wind Turbine Driving a DFIG *IEEE Trans. on Power Electronics*, 2008, vol. 23, no. 3, pp. 1156-1169.

[8] N. Kalamian, M. Verij Kazemi, and S. Asghar Gholomian, Direct power control of DFIG by using nonlinear model predictive controller, Asian Journal of Control, Vol. 18, No. 3, pp. 985-999 (2016).

[9] Rishabh Dev Shukla, Ramesh Kumar Tripathi, Padmanabh Thakur. DC grid/bus tied DFIG based wind energy system. Renewable Energy 2017;108:179-193.

[10] S.K. Routray, R.K. Patnaik and P.K. Dash, Adaptive Non-Linear Control of UPFC for Stability Enhancement in a Multimachine Power System Operating with a DFIG Based Wind Farm, Asian Journal of Control, Vol. 19, No. 4, pp. 1575-1594, (2017).

[11] B. Beltran, T. Ahmed-Ali, and M.E.H. Benbouzid, High-Order Sliding-Mode Control of Variable-Speed Wind Turbines, *IEEE Trans. Indus. Electro.*, 2009, 56, pp. 3314-3321.

[12] Chaker Zaafouri, Borhen Torchani, Anis Sellami and Germain Garcia, Uncertain Saturated Discrete-Time Sliding Mode Control for A Wind Turbine Using A Two-Mass Model, Asian Journal of Control, Vol. 20, No. 4, pp. 1-17, (2018).

[13] Bo Yang, Tao Yu, Hongchun Shu, Jun Dong, Lin Jiang. Robust sliding-mode control of wind energy conversion systems for optimal power extraction via nonlinear perturbation observers. Applied Energy. 2018;210:711-723.

[14] Maissa Farhat, Oscar Barambones and Lassaad Sbita. A New Maximum Power Point Method Based on a Sliding Mode Approach for Solar Energy Harvesting. Applied Energy. 2017;185:1185-1198.

[15] Yanjun Huang, Amir Khajepour, Haitao Ding, Farshid Bagheri, Majid Bahrami. An energy-saving set-point optimizer with a sliding mode controller for automotive air-conditioning/refrigeration systems. Applied Energy. 2017;188:576-585.

[16] R. Saravanakumar, D. Jena, Nonlinear control of a wind turbine based on nonlinear estimation techniques for maximum power extraction, International Journal of Green Energy , Vol. 13, No. 3, pp. 309-319, (2016).

[17] Fernando Jaramillo-Lopez, Godpromesse Kenne, Francoise Lamnabhi-Lagarrigue, A novel online training neural network-based algorithm for wind speed estimation and adaptive control of PMSG wind turbine system for maximum power extraction, Renewable Energy. 2016;86:38-48

[18] Roberto Fantino, Jorge Solsona, Claudio Busada. Nonlinear observer-based control for PMSG wind turbine. Energy 2016;113:248-257.

[19] Dongran Song, Jian Yang, Zili Cai, Mi Dong, Mei Su, Yinghua Wang. Wind estimation with a non-standard extended Kalman filter and its application on maximum power extraction for variable speed wind turbines. Applied Energy. 2017;190:670-685.

[20] O. Barambones, J.M. Gonzalez de Durana, and P. Alcorta, Wind Turbine Output Power Maximization based on Sliding Mode Control Strategy, *Proceeding of the 2010 IEEE International Sysmposium on Industrial Electronics*, Bari (2010).

[21] O. Barambones, J.M. Gonzalez de Durana, and M. de la Sen, Robust speed control for a variable speed wind turbine, *Innovative Journal of Computing Information and Control*, Vol.11,, pp.7627-7640 (2012).

[22] Fernando D. Bianchi, Hrnan De Battista and Ricardo J. Mantz 2007 *Wind Turbine Control Systems* Advances in Industrial Control Series. Springer.

[23] T.R. Ayodele, A.S.O. Ogunjuyigbe, B.B. Adetokun. Optimal capacitance selection for a wind-driven self-excited reluctance generator under varying wind speed and load conditions. Applied Energy. 2017;190:339-353.

[24] Hamed Moradi, Gholamreza Vossoughi. Robust control of the variable speed wind turbines in the presence of uncertainties: A comparison between H_∞ and PID controllers. Energy 2015;90:1508-1521.

[25] P.V. Kokotovic, H. Khalil, J. OReilly. (1996) Singular Perturbation Methods in Control: Analysis and Design *Academic Press*, New York.

[26] R. Pena, J. C. Clare, and G. M. Asher 1996 Doubly fed induction generator using back-to-back PWM converters and its application to variablespeed wind-energy generation *Proc. Inst. Elect. Eng.*, vol. 143, no. 3, pp. 231-241.

[27] D. W. Novotny and T. A. Lipo, 2000 *Vector Control and Dynamics of AC Drives*. Oxford, U.K.: Oxford Univ. Press, 2000.

[28] Yazhou Lei, Alan Mullane, Gordon Lightbody, and Robert Yacamini 2006, Modeling of the Wind Turbine With a Doubly Fed Induction Generator for Grid Integration Studies, *IEEE Trans. on Energy Conversion*, vol. 21, no. 1, pp. 257-264.

[29] Utkin V.I., 1993, Sliding mode control design principles and applications to electric drives, *IEEE Trans. Indus. Electro.*, 40, 26-36.

[30] Richard Gagnon, Gilbert Sybille, Serge Bernard, Daniel Par, Silvano Casoria, Christian Larose. Modeling and Real-Time Simulation of a Doubly-Fed Induction Generator Driven by a Wind Turbine. International Conference on Power Systems Transients (IPST05) in Montreal, Canada on June 19-23, 2005. Paper No. IPST05-162

[31] Basma Boujoudi, Elmkaddem Kheddioui Nadia Machkour. Comparative study between PI and the sliding mode control for the DFIG of a wind turbine. 2017 14th International Multi-Conference on Systems, Signals & Devices (SSD)

[32] Darya khan Bhutto,.Jamshed Ahmed Ansari, Faheem Chachar,.Sunny Katyara,Jahangeer Soomro. Selection of optimal controller for active and reactive power control of doubly fed induction generator (DFIG). 2018 International Conference on Computing, Mathematics and Engineering Technologies iCoMET 2018.